Neurosci. Bull. May, 2022, 38(5):474–488
https://doi.org/10.1007/s12264-021-00782-w

www.neurosci.cn
www.springer.com/12264

ORIGINAL ARTICLE

Entrainment of Astrocytic and Neuronal Ca^{2+} Population Dynamics During Information Processing of Working Memory in Mice

Zhu Lin[1] · Feng You[1] · Ting Li[1] · Yijia Feng[1] · Xinyue Zhao[1] · Jingjing Yang[1] · Zhimo Yao[1] · Ying Gao[1] · Jiang-Fan Chen[1]

Received: 16 April 2021 / Accepted: 27 July 2021 / Published online: 26 October 2021
© Center for Excellence in Brain Science and Intelligence Technology, Chinese Academy of Sciences 2021

Abstract Astrocytes are increasingly recognized to play an active role in learning and memory, but whether neural inputs can trigger event-specific astrocytic Ca^{2+} dynamics in real time to participate in working memory remains unclear due to the difficulties in directly monitoring astrocytic Ca^{2+} dynamics in animals performing tasks. Here, using fiber photometry, we showed that population astrocytic Ca^{2+} dynamics in the hippocampus were gated by sensory inputs (centered at the turning point of the T-maze) and modified by the reward delivery during the encoding and retrieval phases. Notably, there was a strong inter-locked and antagonistic relationship between the astrocytic and neuronal Ca^{2+} dynamics with a 3-s phase difference. Furthermore, there was a robust synchronization of astrocytic Ca^{2+} at the population level among the hippocampus, medial prefrontal cortex, and striatum. The inter-locked, bidirectional communication between astrocytes and neurons at the population level may contribute to the modulation of information processing in working memory.

Keywords Working memory · Ca^{2+} dynamics · Astrocyte · Neuron · Fiber photometry · Hippocampus

✉ Ying Gao
gaoying105@163.com

✉ Jiang-Fan Chen
chenjf555@gmail.com

[1] The Molecular Neuropharmacology Laboratory and the Eye-Brain Research Center, State Key Laboratory of Ophthalmology, Optometry and Visual Science, School of Optometry and Ophthalmology and Eye Hospital, Wenzhou Medical University, Wenzhou 325035, China

Introduction

Astrocytes not only provide metabolic support and homeostatic control but are also increasingly recognized to play an active role in various traditionally neuron-centered cognitive processes, including learning and memory [1–7]. Genetic knockout and pharmacological manipulations of inositol 1,4,5-triphosphate receptors (IP3Rs) and other astrocytic G-protein-coupled receptors have uncovered essential roles of astrocytes in the modulation of cognition, including working memory (WM) [8, 9], hippocampus-dependent spatial memory [10, 11], emotional behaviors [12, 13], and sleep and arousal regulation [14]. Astrocytes are in close proximity to neurons and can sense local neural activity and brain-wide neuromodulatory inputs and contribute to these cognitive processes *via* bidirectional interactions between astrocytes and synapses as components of tripartite synapses [15–17]. Astrocytes also show characteristic Ca^{2+} activity in responses to sensory [18] and motor events [19] and evoke the Ca^{2+}-dependent release of gliotransmitters [20–22]. Dysregulation of Ca^{2+} dynamics *in vivo* contributes to neurological diseases such as epilepsy and Alzheimer's disease [23]. Understanding Ca^{2+} dynamics is critical to elucidating the role of astrocytes in physiological and pathological processes.

Astrocytic Ca^{2+} dynamics *in vivo* have been studied with two-photon microscopy and camera-based large-field imaging, but these studies are limited by imaging of cortical layers [24], by using anesthetized animals (which may alter neural responses) [25], and by using head-fixed awake mice, which introduce stress to alter astrocytic function [19, 26]. The exact dynamic role of astrocytes in these cognitive processes remains unclear due to the difficulties in directly and specifically recording the astrocytic Ca^{2+} dynamics in animals performing tasks.

The recent development of genetically-encoded Ca^{2+} indicator (GECI)-based fiber photometry enables the recording of intracellular Ca^{2+} signal in defined cells of behaving (task-performing) animals and provides a new opportunity to correlate the astrocytic Ca^{2+} signal with specific cognitive processes [27–29]. Recent studies using GECIs have shown that the astrocytic Ca^{2+} signal can be triggered by sensory [18], odor [30], and visual [31] stimulation, as well as by locomotion and startle responses [32]. However, whether these sensory and neural inputs can trigger event-specific astrocytic Ca^{2+} patterns to participate in specific cognitive processes remains unknown. Specifically, it is unknown whether specific patterns of astrocytic Ca^{2+} dynamics may exist and be embedded in neural circuits in association with specific cognitive processes. If such a pattern exists, what information does it encode, and how does it specifically correlate with neuronal network activity?

WM is characterized by temporary storage and manipulation of information to instruct a behavioral response, and is the foundation of cognitive behaviors [33]. Previous studies on WM have mainly focused on the neurons or neuronal networks in control of WM processing [34–36]. Many pharmacological and genetic-knockout studies have also demonstrated the astrocytic modulation of WM [9, 37, 38]. For example, astrocytes can control WM by modulating their release of D-serine to "boost" the induction of long-term potentiation (LTP) [39], by providing astrocyte-derived L-lactate to enhance LTP as metabolic fuel for synaptic remodeling to influence rule-learning and the performance of WM [38, 40], and by cannabinoid receptor type-1 signaling *via* inhibition of transmitter release at GABAergic and glutamatergic terminals [8]. However, as these experimental manipulations of astrocyte activity result in long-term activity changes in astrocytes, whether specific patterns of astrocytic Ca^{2+} dynamics may exist in association with specific WM processing (at the time scale of seconds) remains unclear. In particular, WM processing consists of three distinct information-processing phases, encoding, maintenance, and retrieval, and each phase can be completed within a few seconds [41]. Indeed, the hippocampus → prefrontal cortex (PFC) neural pathway is critical for the encoding of spatial WM [42], while the PFC is essential for the maintenance of WM [36], and the thalamus and striatum are involved in the retrieval of WM [43]. To the best of our knowledge, there is no information on astrocytic Ca^{2+} dynamics during the distinct phases of WM, and, consequently, whether astrocytes temporally participate in these distinct phases of WM processing in real time remains unknown. Furthermore, emerging studies have shown the dynamic interactions between astrocytes and neurons in animals responding to different stimuli [30, 31, 44]. However, the question whether astrocytes can dynamically and temporally precisely interact with neurons at the population level during WM processing remains to be answered. Lastly, WM processing reportedly involves many brain regions, including the hippocampus (encoding phase), medial PFC (mPFC) (maintenance phase), and striatum (maintenance and retrieval phases) [45, 46], with the communications of neuronal networks among these WM-related regions [46, 47]. Whether there is communication, such as synchronization, of astrocytic Ca^{2+} networks among these WM-related regions [48, 49] is currently unclear.

Therefore, we designed experiments to elucidate the dynamic role of astrocytic Ca^{2+} at the population level in the distinct information processes of WM by coupling GECI-based fiber photometry with the T-maze-based delay-no-match-to-place WM task. While the mPFC is critical to the maintenance of WM, we focused on astrocytic Ca^{2+} in the hippocampus, since astrocytic Ca^{2+} is strongly triggered by sensory inputs, and this is most evident in the encoding and retrieval phases [50], and the hippocampus → cortex pathway is critical to the encoding of WM information processing [42]. Our analysis revealed the gating of astrocytic Ca^{2+} dynamics by sensory inputs and the internal state, a strong inter-locked and antagonistic relationship between the astrocytic and neuronal Ca^{2+} dynamics, and the synchronization of astrocytic Ca^{2+} signals responding to WM processing between the hippocampus, mPFC, and striatum. These findings support the existence of bidirectional and inter-locked communication between astrocytes and neurons at the population level to fine-tune the WM information processing.

Materials and Methods

Animals

The animal protocols were approved by the Institutional Ethics Committee for Animal Use in Research and Education at Wenzhou Medical University, China. Male C57BL/6 J mice aged 8 weeks were purchased from SPF Biotechnology Co., Ltd (Beijing, China), and housed at 24 ± 0.5 °C with a relative humidity of 60% ± 2% and under a 12-h light-dark cycle (lights on at 08:00). Except when food-restricted for behavioral training and testing, all mice were given *ad libitum* access to food and water.

Stereotaxic AAV Injection and Optic Fiber Implantation

The stereotaxic AAV injection and optic fiber implantation were performed as described previously [43]. Briefly, for

the dual-color fiber photometry experiment, male C57BL/6J mice (aged 8–12 weeks) were intraperitoneal anesthetized with sodium pentobarbital (50 mg/kg, Boyun, Shanghai, China). Then they were injected with 300 nL of AAV2/9-shortGFAP-Gcamp6s and 300 nL of AAV2/9-hSyn-jRGECO1a simultaneously into the hippocampus [anteroposterior (AP), −2.4 mm from Bregma; mediolateral (ML), −1.75 mm; dorsoventral (DV), −1.3 mm] unilaterally. For the multichannel fiber photometry experiment, male C57BL/6J mice (aged 8–12 weeks) were simultaneously injected with 300 nL of AAV2/9-short-GFAP-Gcamp6(s) into the mPFC (AP, +1.96 mm; ML, −0.35 mm; DV, −1.65 mm), striatum (AP, +0.98 mm; ML, +1.60 mm; DV, −2.60 mm), and hippocampus (AP, −2.4 mm; ML, −1.75 mm; DV, −1.3 mm) unilaterally. The injection rate was 50 nL per min. Optical fibers (Hangzhou Newdoon Technology Co., Ltd, Hangzhou, China, outside diameter: 1.25 mm, core: 200 μm, numerical aperture: 0.37) were implanted 0.1 mm above the injection site. The viruses used in this study were from Obio Technology Co., Ltd (Shanghai, China) and had titers from 1.29×10^{13} to 1.69×10^{13} genome copies per mL. The behavioral tests were started 3–4 weeks after stereotaxic surgery to achieve sufficient virus expression.

T-maze-Based Delayed-Non-Match-to-Place (DNMTP) Task

The T-maze–based DNMTP task was conducted according to the protocol described previously [43]. Briefly, after expression of the AAV2/9 virus for ~3 weeks, mice were first subjected to food restriction for 3 days and then to habituation for another 3 days. The mice were then given 10 trials of training per day for the WM task. During the training and testing periods, the mice were also maintained under food restriction to keep their body weight at 85% of that before training. Each trial consisted of three phases: sample, delay, and choice phases, corresponding to the encoding, maintenance, and retrieval phases of WM, respectively. In the sample phase, one of the two reward arms was randomly blocked, and the mice ran for a food reward from the starting arm to the reward arm (encoding). In the delay phase, the mice were driven to return to the starting arm and maintain the information on the reward arm in the sample phase for a variable delay (such as 10 s) (maintenance). In the choice phase, the blocking wall was removed, and if the mice selected the previously closed arm to achieve a second food reward (retrieval), then this was considered to be a correct trial. However, if the mice selected the previously explored arm without achieving another reward, then this was recorded as a false trial. The final performance of the mice per day was the average correct rate of 10 trials. The mice underwent the training and testing of WM for 4 days to achieve > 80% accuracy in the task. After full acquisition of the task, the mice were then subjected to WM testing with an increasing delay time (from 10 to 20 s, 30 s, and 60 s) during the maintenance phase.

Fiber Photometry Recording and Ca^{2+} Signal Analysis

The dual-color and multichannel fiber photometry system (Thinker Tech Nanjing Bioscience Inc., Nanjing, China) and MatLab (Math Works, Natick, USA) data analysis with custom-written programs were applied according to the manufacturer's instructions. In Ca^{2+} signal analysis during the WM task, we mainly captured the Ca^{2+} dynamics at three event-related time points: (A) when the mice reached the reward arm in the encoding phase; (B) when the mice returned to the start arm at the beginning of the maintenance phase; (C) when the mice reached the reward arm in the retrieval phase. The Ca^{2+} signal values (ΔF/F) were calculated as $(F-F_0)/F_0$, where F_0 is the baseline Ca^{2+} signal when the mice stayed at the start arm or before running (2-s time window). Then, we recorded the Ca^{2+} signal ranging from 8 s before and 10 s after the events.

Histology and Fluorescence Imaging

Briefly, mice were deeply anesthetized and transcardially perfused with 4% paraformaldehyde after optic fiber recording. Then, the brains were removed, post-fixed in 4% paraformaldehyde for 4–6 h, and dehydrated in 30% sucrose for 2–3 days. Coronal sections (30 μm) around the fiber implantation sites were prepared and stained as described previously [43]. Briefly, the sections were blocked at room temperature for 1 h in 10% normal donkey serum, 1% bovine serum albumin, and 0.3% Triton X-100 in phosphate buffered saline (PBS) and incubated with primary antibodies overnight at 4°C (rabbit anti-NeuN, 1:400, Sigma, St. Louis, USA; mouse anti-S100β, 1:400, Sigma). The sections were rinsed in PBS, followed by incubation with the corresponding secondary antibodies (donkey anti-rabbit 488/594, 1:1000, Invitrogen, Carlsbad, USA and donkey anti-mouse 647, 1:1000, Invitrogen). Images were acquired with a fluorescence microscope (LSM 880; Carl Zeiss, Jena, Germany) using a 20× objective.

Statistical Analysis

The quantitative data are presented as the mean ± SEM, analyzed with GraphPad Prism 6 (San Diego, USA). All statistical tests were performed with IBM SPSS Statistics 25 (Chicago, USA). The quantitative differences between

the Ca^{2+} patterns were compared using an independent two-sample *t*-test. The cross-correlation analysis between astrocytic and neuronal Ca^{2+} signals was done with MatLab software (Math Works). The level of statistical significance was set at $P < 0.05$.

Results

Three Astrocytic and Neuronal Ca^{2+} Peaks During the Encoding, Maintenance, and Retrieval Phases of WM

To investigate the real-time astrocytic and neuronal Ca^{2+} dynamics during distinct WM information processing, we coupled GECI-based dual-color fiber photometry with the T-maze-based DNMTP WM task to simultaneously monitor astrocytic and neuronal activity in the hippocampus of mice performing the WM task using a green astrocytic Ca^{2+} indicator (AAV2/9-shortGFAP-GCaMP6s) and a red neuronal Ca^{2+} indicator (AAV2/9-hSyn-jRGECO1a). The GCaMP6s and jRGECO1a immunofluorescence was specifically observed in the hippocampus (Fig. 1A). The Gcamp6s expression almost co-localized with the astrocytic marker S-100β (Fig. 1B, C) and the jRGECO1a expression pattern was similar to that of the neuronal marker NeuN (Fig. 1D, E), confirming the specific astrocytic and neuronal expression patterns of the two Ca^{2+} indicators.

By analyzing the astrocytic and neuronal Ca^{2+} during the WM task, we observed that both astrocytic and neuronal Ca^{2+} exhibited specific patterns responding to the distinct phases of WM processing (Fig. 2A): (1) during the encoding phase, the astrocytic Ca^{2+} signal elevated when the mice approached the reward arm and peaked at the point of obtaining/retrieving the reward; the peak decreased immediately after obtaining the reward but started to increase again when the mice left the reward arm and returned to the start arm; (2) the signal peaked at the starting point of the maintenance phase when the mice arrived at the start arm and then immediately started to decrease and continued to decline (below the baseline) through 10–20 s of the maintenance phase; and (3) the pattern of the signal in the retrieval phase was mainly similar to that in the encoding phase. And we found the decay time of astrocytic Ca^{2+} in the encoding and retrieval phases was significantly shorter than that in maintenance phase (Fig. 2D, E).

Meanwhile, the neuronal Ca^{2+} signal exhibited distinct patterns during the three phases of WM (Fig. 2A): (1) during the encoding phase, the neuronal Ca^{2+} signal rose when the mice approached the turning point, peaked at the turning point, and decreased rapidly before reaching the reward arm; (2) during the maintenance phase, the signal remained at the baseline within 10–20 s; and (3) the signal in the retrieval phase was also similar to that of the encoding phase. We also found that the neuronal Ca^{2+} activity in maintenance phase (staying at the start arm) was significantly higher than that in encoding and retrieval phases (staying at the reward arm) (Fig. 2F, G). Thus, hippocampal astrocytes and neurons displayed distinct Ca^{2+} signal patterns during the three phases of WM, with astrocytic Ca^{2+} peaking at reward arms and neuronal Ca^{2+} peaking at the turning point during the encoding and retrieval phases and with astrocytic Ca^{2+} activity persistently decreasing and neuronal Ca^{2+} remaining constant during the maintenance phase.

We also analyzed the astrocytic and neuronal Ca^{2+} signals during high WM-loading periods with 20-s, 30-s, and 60-s delay times (Fig. 3). Both astrocytic and neuronal Ca^{2+} patterns in the encoding and retrieval phases were almost the same as in the 10-s delay time. With a prolonged delay phase, the astrocytic Ca^{2+} signal persistently decreased below the baseline for 20 s and then returned to the baseline level for the rest of delay time (up to 60 s). However, neuronal Ca^{2+} largely remained constant at the baseline level for $\sim$ 30 s.

As astrocytic Ca^{2+} signals can be triggered by sensory stimulation, startle responses [18, 32], or locomotion [19, 51], it was difficult to separate the different components that trigger the specific patterns of astrocytic Ca^{2+} signals since the WM task involves multiple simultaneous inputs. However, when we recorded the astrocytic and neuronal Ca^{2+} signals simultaneously while the mice were in the home cage or during habituation in the T-maze, we did not observe any specific patterns in these two states (Fig. 1F, G).

Bidirectional and Inter-Locked Interaction Between Astrocytic and Neuronal Ca^{2+} During Information Processing of WM

We further analyzed the relationships between astrocytic and neuronal Ca^{2+} in the distinct phases of WM processing by constructing hysteresis loops (Fig. 2B). The hysteresis loop analysis revealed that neuronal Ca^{2+} increased initially and this was followed by the continuous elevation of astrocytic Ca^{2+}, with an accompanying decrease in neuronal Ca^{2+}. Lastly, neuronal Ca^{2+} increased again with the decay of astrocytic Ca^{2+}. Furthermore, cross-correlation analysis indicated that astrocytes not only positively correlated to neurons with a delay of $\sim$ 3 s, but also negatively correlated to neurons with a preceding time of $\sim$3 s during the WM task (Fig. 2C). So, interestingly, both the delay and preceding times of astrocytic Ca^{2+} dynamics relative to neurons were $\sim$ 3 s. In addition, the correlation

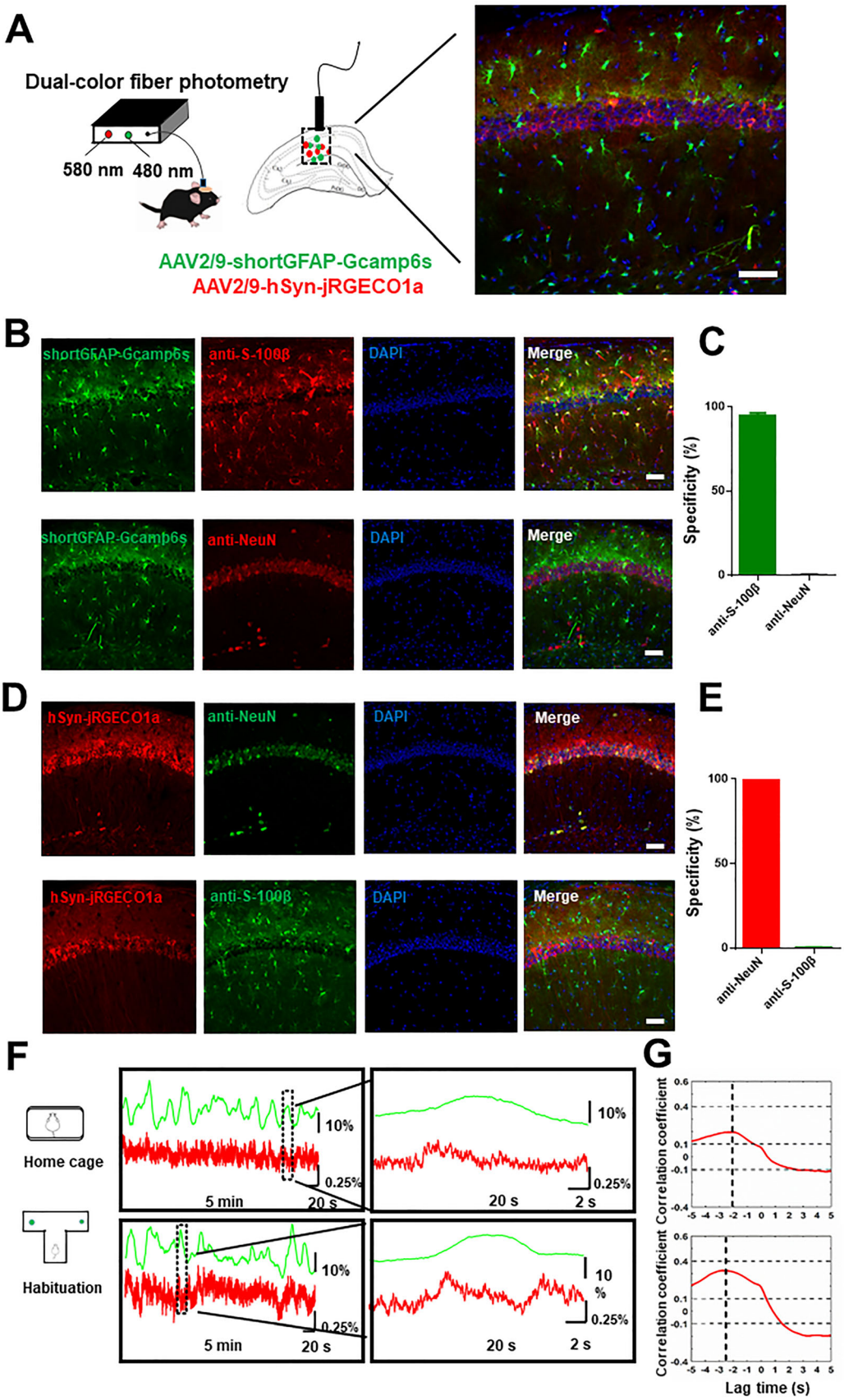
A
Dual-color fiber photometry
580 nm 480 nm
AAV2/9-shortGFAP-Gcamp6s
AAV2/9-hSyn-jRGECO1a
B
shortGFAP-Gcamp6s
anti-S-100β
DAPI
Merge
shortGFAP-Gcamp6s
anti-NeuN
DAPI
Merge
C
Specificity (%)
100
50
0
anti-S-100β
anti-NeuN
D
hSyn-jRGECO1a
anti-NeuN
DAPI
Merge
hSyn-jRGECO1a
anti-S-100β
DAPI
Merge
E
Specificity (%)
100
50
0
anti-NeuN
anti-S-100β
F
Home cage
Habituation
10%
0.25%
5 min
20 s
20 s
2 s
10%
0.25%
5 min
20 s
20 s
2 s
10 %
0.25%
G
Correlation coefficient
Correlation coefficient
Lag time (s)

◀**Fig. 1** Dual-color fiber photometry recording of astrocytic and neuronal Ca^{2+} signals in the hippocampus. **A** Schematic of dual-color fiber photometry to record astrocytic and neuronal Ca^{2+} signals by simultaneously expressing AAV2/9-shortGFAP-Gcamp6s (green) and AAV2/9-hSyn-jRGECO1a (red) in the hippocampus (scale bar, 50 μm). AAV2/9, adeno-associated virus type 2/9. **B, C** Representative images (**B**; scale bar, 50 μm) and statistics (**C**; mean ± SEM; n = 3 mice) showing the Ca^{2+} indicator Gcamp6s (green) is co-localized with the astrocytic marker S-100β (red) but minimally with the neuronal marker NeuN (red). **D, E** Representative images (**D**; scale bar, 50 μm) and statistics (**E**; mean ± SEM; n = 3 mice) showing the Ca^{2+} indicator jRGECO1a (red) is specifically co-localized with the neuronal marker NeuN (green) but not with the astrocytic marker S-100β (green). **F** Example traces of astrocytic (green) and neuronal Ca^{2+} (red) during behavior in the home cage and during habituation. **G** Averaged correlation coefficients of astrocytic and neuronal Ca^{2+} in the home cage and during habituation.

analysis [52] of astrocytic and neuronal Ca^{2+} signals indicated a slight correlation during the home cage state and a weak positive correlation during habituation to the T-maze (Fig. 1G). Collectively, these analyses indicate bidirectional interactions and coordination between astrocytic and neuronal networks contributing to WM processing.

Rule Learning in WM Produces Plasticity Changes in the Astrocytic and Neuronal Ca^{2+} Dynamics

As the training proceeded, the WM performance improved by increasing the correct trial rate (Fig. 4A). To explore whether astrocytes are involved in modulating WM performance, we compared astrocytic Ca^{2+} activity between correct and wrong trials in the WM task (Fig. 4B). During the retrieval phase, astrocytic Ca^{2+} activity in the wrong trials was significantly higher than in the correct trials on day 3 (Fig. 4D) and day 4 (Fig. 4F). But during the encoding phase, astrocytic Ca^{2+} activity in the wrong trials was significantly weaker than in the correct trials on day 4 (Fig. 4E). Similarly, we also compared neuronal Ca^{2+} activity between the correct and wrong trials in the WM task (Fig. 4C). The results show that neuronal Ca^{2+} activity in the retrieval phase of the wrong trials was significantly higher than in the correct trials during day 2 (Fig. 4G) and day 3 (Fig. 4H). So, the main differences in astrocytic and neuronal Ca^{2+} signals between correct and wrong trials occurred on day 3 when the mice started to achieve good performance, suggesting a modulatory role of astrocytes in WM performance after rule learning.

To further determine whether astrocytic Ca^{2+} exhibits plasticity with rule learning in the WM task, we analyzed astrocytic Ca^{2+} transients in 4 training days. When WM performance increased after 4 training days (Fig. 4A), astrocytic Ca^{2+} activity exhibited plasticity changes (Fig. 5A). Astrocytic Ca^{2+} dynamics increased in the maintenance phase (Fig. 5C) and decreased in the retrieval phase (Fig. 5D) on training days 2–4 compared to day 1. Moreover, we found similar plasticity changes of neuronal Ca^{2+} activity at 4 training days (Fig. 5E): neuronal Ca^{2+} dynamics increased in the maintenance phase (Fig. 5G) and tended to decrease in the retrieval phase (Fig. 5H) on training days 2–4 compared to day 1. In the second part of the encoding phase, astrocytic Ca^{2+} activity increased (Fig. 5B) while neuronal Ca^{2+} dynamics decreased over 4 training days compared to day 1 (Fig. 5F). These results indicate that astrocytic and neuronal Ca^{2+} exhibit plasticity changes during WM processing.

Synchronization and Heterogeneity of Astrocytic Ca^{2+} Dynamics During Information Processing of WM in the Hippocampus, mPFC, and Striatum

To explore astrocytic Ca^{2+} signals in other WM-related brain regions, we applied multichannel fiber photometry to monitor the dynamics of astrocytic Ca^{2+} in the mPFC, striatum, and hippocampus simultaneously during the WM task (Fig. 6A). First, the astrocytic Ca^{2+} dynamics from the three regions were synchronized both during free movement (Fig. 6B) and performance of the WM task (Fig. 6D). Correlation of the dynamics between the hippocampus and mPFC, or between the hippocampus and striatum was > 0.6 (Fig. 6C), suggesting the synchronization of astrocytic Ca^{2+} among WM-related brain regions.

However, astrocytic Ca^{2+} in the three brain regions also displayed heterogeneity during WM processing (Fig. 6E): (1) during the encoding phase, astrocytic Ca^{2+} activity in the mPFC and hippocampus was significantly stronger than in the striatum; (2) during the maintenance phase, the activity in the hippocampus and striatum was stronger than in the mPFC; and (3) during the retrieval phase, the activity in the mPFC was higher than in the striatum. Taken together, these results not only demonstrated the existence of astrocytic Ca^{2+} synchronization in distinct WM-related regions but also showed the heterogeneity of the astrocytic Ca^{2+} dynamics in distinct brain regions during information processing of WM.

Discussion

One of the central issues is to identify specific astrocytic Ca^{2+} patterns in relation to the distinct phases of WM (such as encoding, maintenance, and retrieval), specific location in space, emotional state (reward experience/delivery), and memory acquisition (such as rule learning), such that the population Ca^{2+} dynamics in astrocytes contribute to real-time information processing of WM. Our online monitoring of the astrocytic and neuronal Ca^{2+}

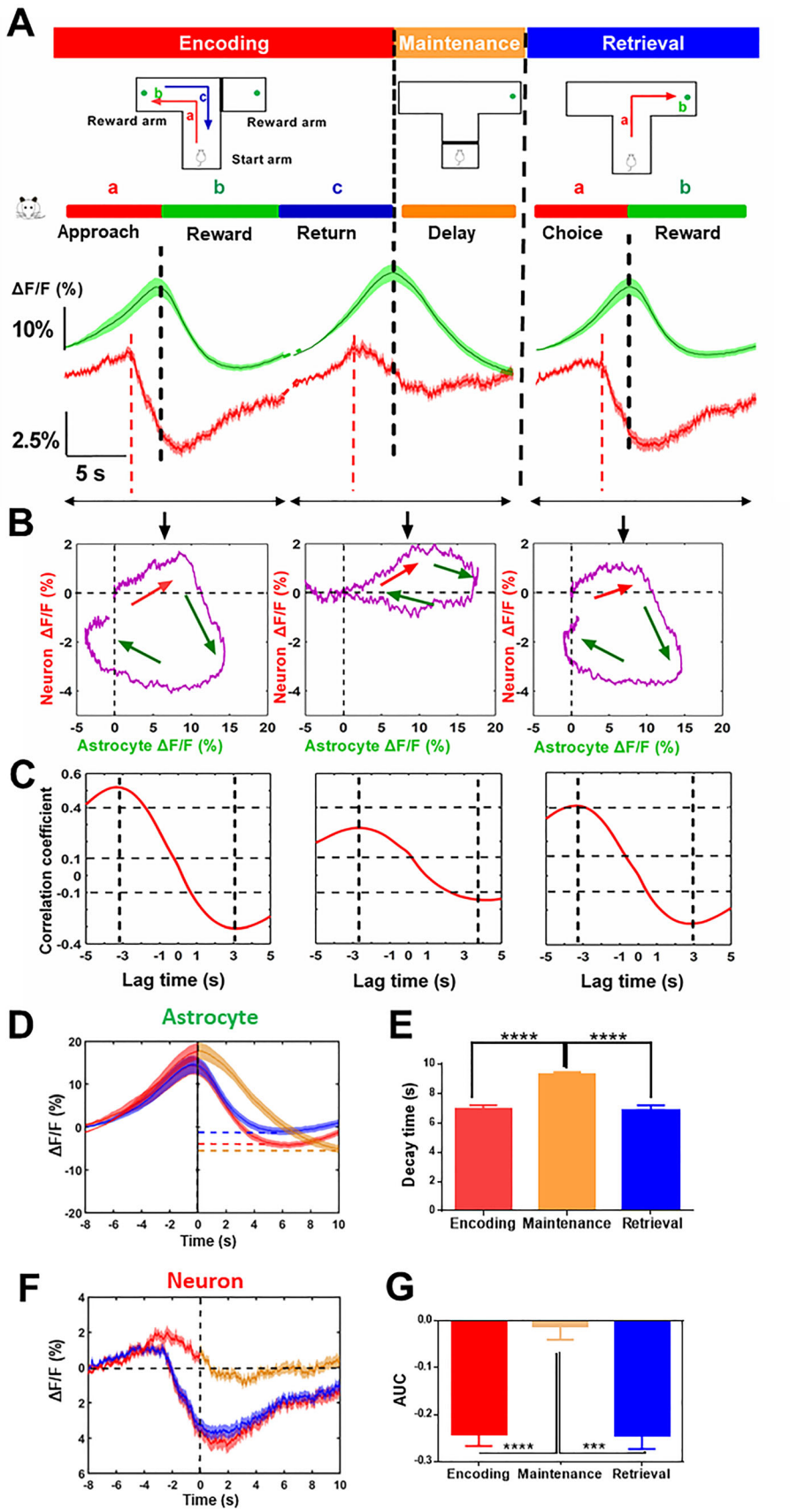

Fig. 2 Specific patterns of astrocytic and neuronal Ca^{2+} responses to WM processing. **A** Schematic of the T-maze-based DNMTP WM task, divided into encoding, maintenance, and retrieval phases. Astrocytic (green) and neuronal Ca^{2+} (red) signals are simultaneously recorded during these phases of WM (red dashed line, mouse arrives at the turning point; black dashed line, mouse arrives at the reward arm). **B** Hysteresis loops between neuronal and astrocytic Ca^{2+} activity, showing that the astrocytic activity increases following an increment in neuronal Ca^{2+} (red arrow) followed by the decrement of neuronal Ca^{2+} activity (green arrow). **C** Analysis of correlation coefficients between astrocytic and neuronal Ca^{2+} corresponding to the three transients above. **D, E** Astrocytic Ca^{2+} transients (**D**) and the decay time of Ca^{2+} signal (**E**) among the three phases of WM. **F, G** Neuronal Ca^{2+} transients (**F**) and the area under the curve (AUC) of Ca^{2+} activity (**G**) among the three phases of WM. The average traces of astrocytic Ca^{2+} and neuronal Ca^{2+} are each from 80 trials (8 mice). The shaded area represents SEM. $^{***}P < 0.001$; $^{****}P < 0.0001$; Tukey's multiple comparisons test.

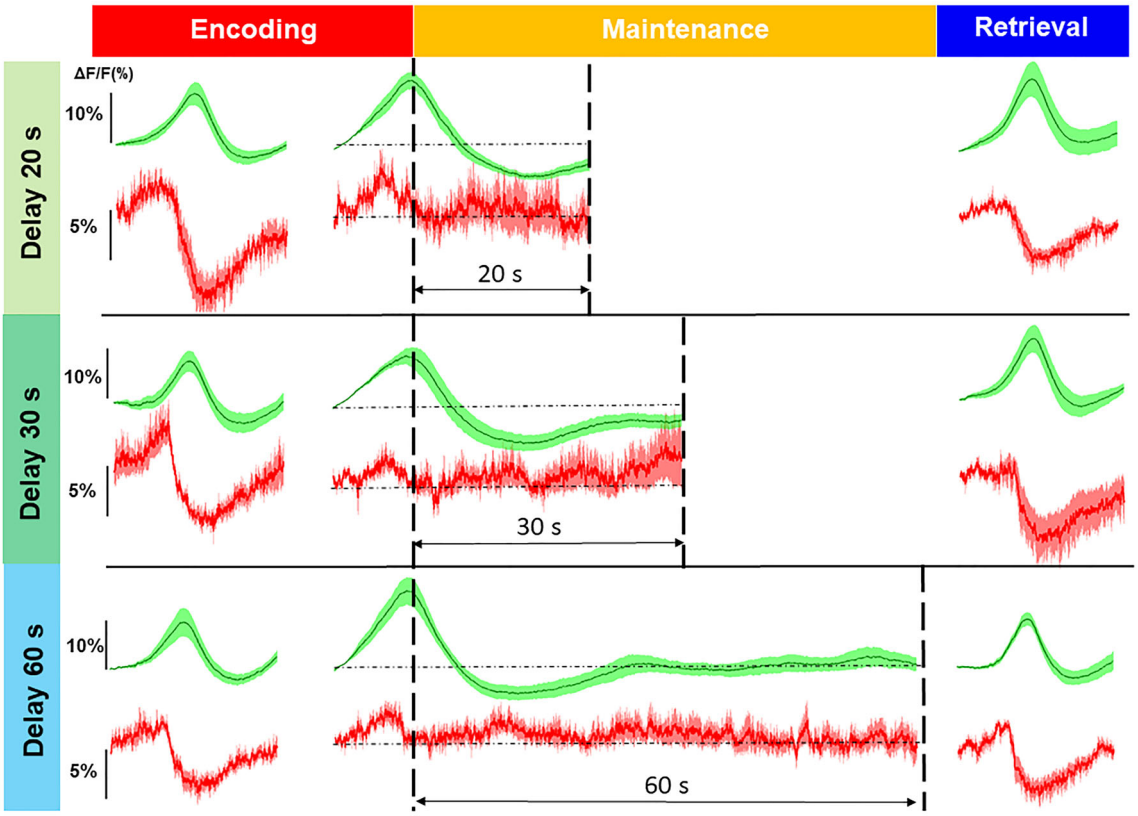

Fig. 3 Dynamic transients of astrocytic and neuronal Ca^{2+} in the three phases of WM processing when the decay time is 20 s, 30 s, or 60 s. The average traces of astrocytic Ca^{2+} (green) and neuronal Ca^{2+} (red) are each from 80 trials (8 mice). The shaded area represents the SEM. The vertical scale bars represent 10% and 5% as indicated.

dynamics of animals performing a WM task provides the first analysis of the dynamic interaction of astrocytic and neuronal networks at the population Ca^{2+} level during distinct phases of WM. The most notable pattern of the astrocytic population Ca^{2+} signal was the three distinct Ca^{2+} peaks during the encoding and retrieval phases associated with the animal's approach to the turning point in the T-maze (the decision-making point) and the inter-locked, antagonistic relationship with the neuronal Ca^{2+} dynamics at a characteristic 3-s phase difference during WM information processing.

Astrocyte Ca^{2+} Dynamics are Gated by Sensory Inputs and Modified by Reward Experience

The notable three astrocytic Ca^{2+} peaks in the encoding and retrieval phases were all spatially associated with the T-maze turning point; the onset of the astrocytic and neuronal Ca^{2+} peaks correlated with the animals' approaching and returning to the turning point of the T-maze. While the neuronal Ca^{2+} signal peaked at the turning point location, astrocytic Ca^{2+} continued to increase until the animals reached the reward. The turning point may represent a (spatial) sensory input that evokes Ca^{2+} signals in astrocytes and neurons. Consistent with this, whisker stimulation triggers a transient increase in noradrenaline and, consequently, a transient Ca^{2+} rise in astrocytes in rodents [32], whereas repeated aversive stimulation produces sustained adrenergic release and increased levels of intracellular Ca^{2+} and cAMP in a large population of astrocytes [53]. The "place cells" in the hippocampus fire in unique sequences forming rhythmic activity such as theta oscillations when the animal is in specific locations, thus encoding critical spatial information [54]. It has been speculated that astrocytic Ca^{2+} responds to the "place cell" rhythmic activity and works in concert with neurons to encode spatial information during WM processing. Besides, delayed astrocyte activity can be triggered by a surge of neuronal network activity in the gamma range (30–50 Hz) induced by sensory stimuli [55]. Thus, the astrocytic Ca^{2+} dynamics may be triggered by neural activity of the place cells or neural rhythmic change of neurons in the hippocampus at this specific turning point of the T-maze. Alternatively, the turning point may also represent a decision-making point since the mice need to use specific spatial information to guide them to the reward at this point. Furthermore, these sensory-elicited astrocytic Ca^{2+} dynamics were further modified by the internal state

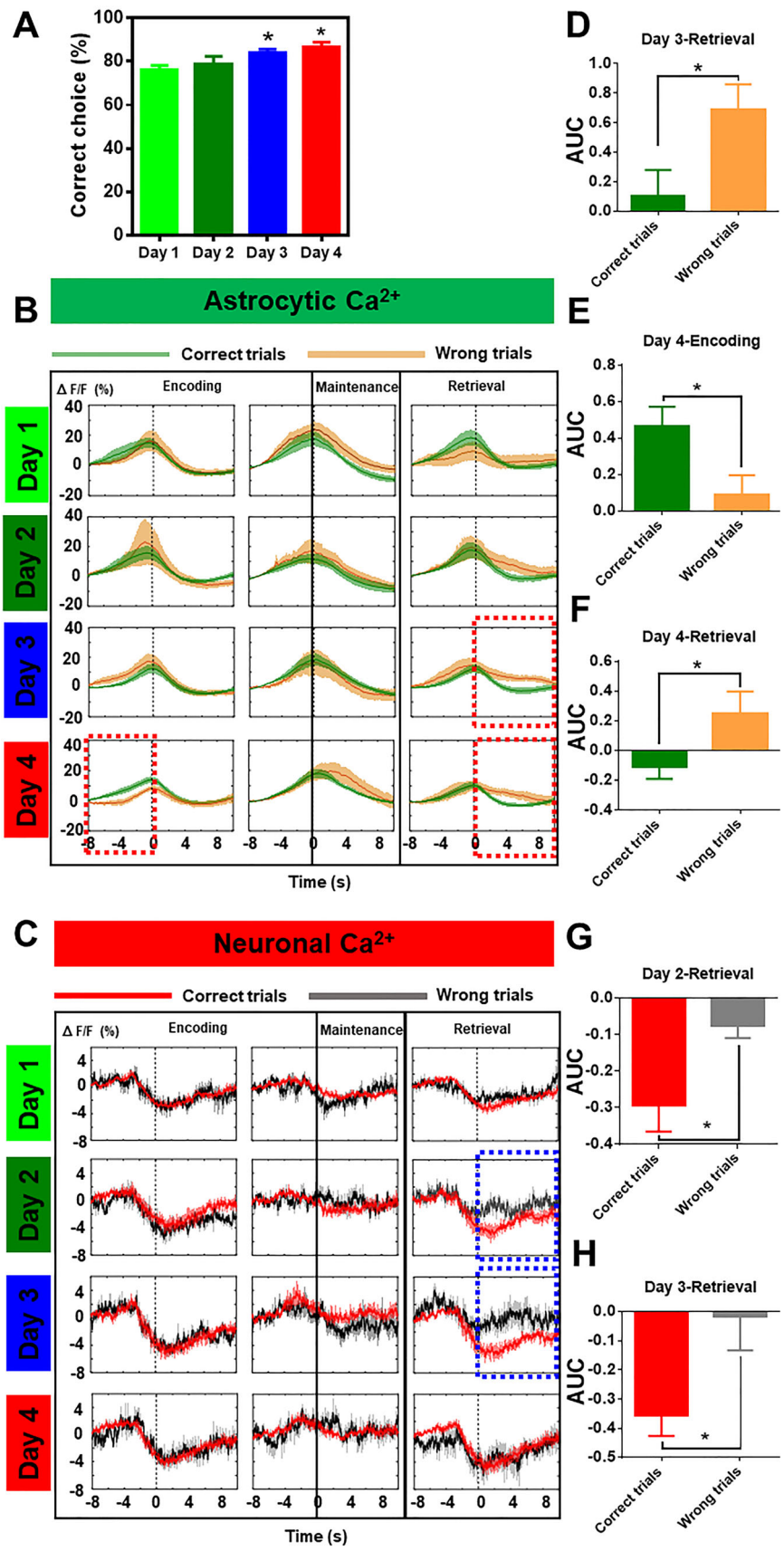

Fig. 4 Comparison of astrocytic and neuronal Ca^{2+} signals between the correct and wrong trials. **A** Performance of virus-injected mice in the T-maze-based WM task during the four days of training. **B** Averaged astrocytic Ca^{2+} transients in the correct trials (green) and wrong trials (orange) corresponding to the three phases of WM on each of the four training days (n = 8 mice; shaded area, SEM). **C** Averaged neuronal Ca^{2+} transients in the correct trials (red) and wrong trials (grey) corresponding to the three phases of WM during each of the 4 training days (n = 8 mice; shaded area, SEM). **D–F** AUC for astrocytic Ca^{2+} activity indicated in the dashed boxes in (**B**). **G, H** AUC for neuronal Ca^{2+} activity indicated in the dashed boxes in (**C**). The numbers of correct trials were 61 on day 1; 63 on day 2; 67 on day 3; 71 on day 4, and the numbers of wrong trials were 19 on day 1; 17 on day 2; 13 on day 3; 9 on day 4. *$P < 0.05$, paired-sample t-test. AUC, area under the curve.

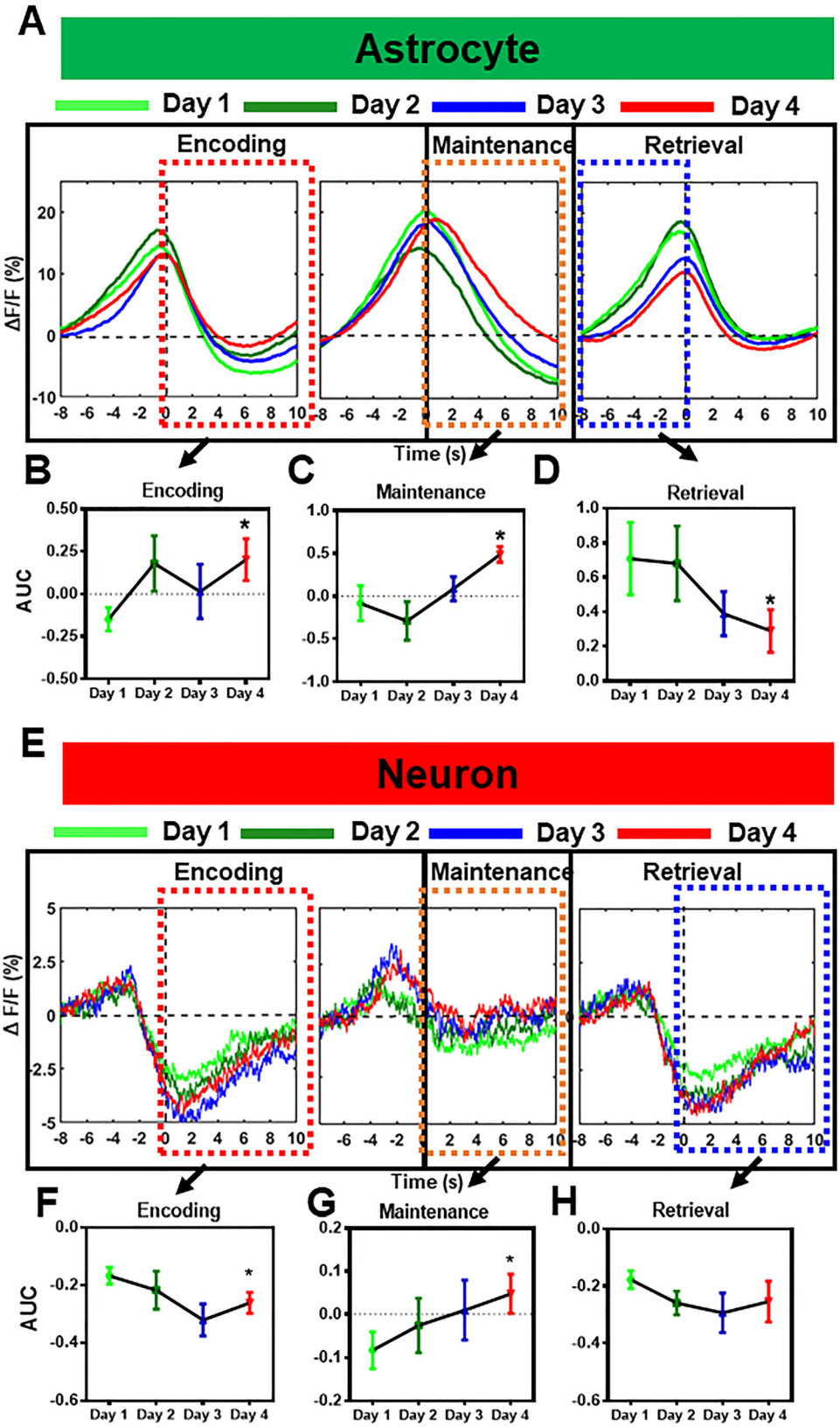

Fig. 5 The astrocytic Ca^{2+} signal exhibits plasticity with rulelearning during the WM task. A Astrocytic Ca^{2+} transients corresponding to the 3 phases of WM among the 4 training days. **B–D** AUC for astrocytic Ca^{2+} activity indicated in the dashed boxes in (**A**). **E** Neuronal Ca^{2+} transients corresponding to the three phases of WM among the 4 training days. **F–H** AUC for neuronal Ca^{2+} activity indicated in the dashed boxes in (**E**). **P*<0.05, repeated measures one-way ANOVA.

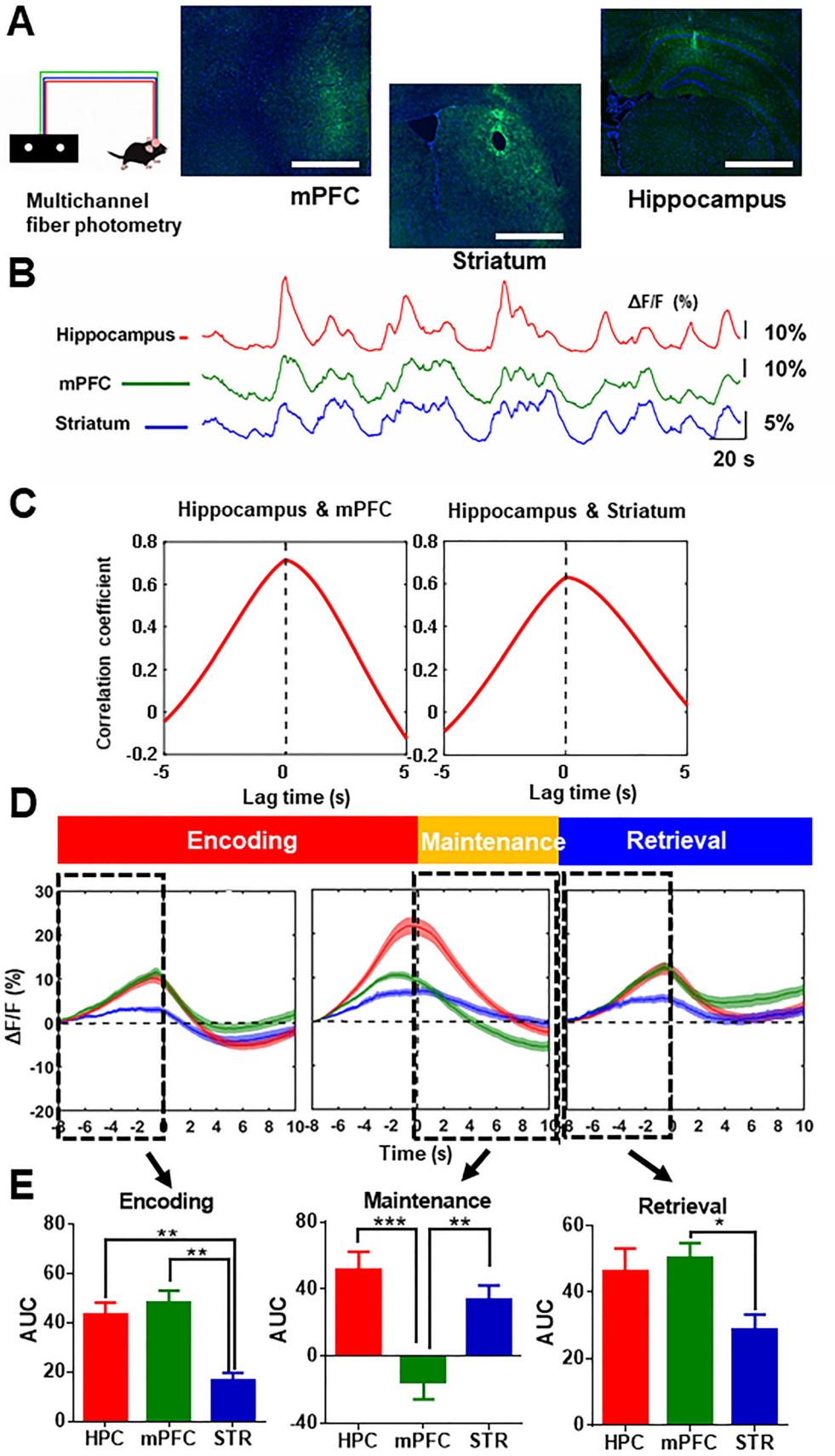
A
Multichannel
fiber photometry
mPFC
Striatum
Hippocampus
B
ΔF/F (%)
Hippocampus
mPFC
Striatum
10%
10%
5%
20 s
C
Hippocampus & mPFC
Hippocampus & Striatum
Correlation coefficient
Lag time (s)
Lag time (s)
D
Encoding
Maintenance
Retrieval
ΔF/F (%)
Time (s)
E
Encoding
Maintenance
Retrieval
AUC
HPC
mPFC
STR

◀**Fig. 6** Synchronization and heterogeneity of astrocytic Ca^{2+} signals responding to WM processing in distinct brain regions. **A** Cartoon of multichannel fiber photometry to record astrocytic signals in the hippocampus, mPFC, and striatum, and the expression of AAV2/9-shortGFAP-Gcamp6s (green) in the three brain regions (scale bars, 1 mm). **B** Representative trials showing simultaneous astrocytic Ca^{2+} transients recorded in the hippocampus (red), mPFC (green), and striatum (blue) in freely-moving mice (vertical bars, 10% and 5%; horizontal bar, 20 s). **C** Correlation coefficients of astrocytic Ca^{2+} corresponding to WM processing the hippocampus and mPFC (left), and the hippocampus and the striatum (right). **D** Dynamic patterns of the averaged astrocytic Ca^{2+} signal in the hippocampus (red), mPFC (green), and striatum (blue) corresponding to distinct phases of WM (10 trials in 9 mice; shaded area, SEM). **E** AUC for astrocytic Ca^{2+} at different WM phases in distinct brain regions, as indicated in the dashed boxes in (**D**). HPC, hippocampus; mPFC, medial prefrontal cortex; STR, striatum. $*P < 0.05$, $**P < 0.01$, $***P < 0.001$, Tukey's multiple comparisons test.

of the animals, such as the reward experience. In particular, we noted that delivery of the reward in the encoding and retrieval phases was associated with a faster decrease in the Ca^{2+} than in the delay phase (without reward). Thus, sensory inputs (spatial information such as the turning point) and internal state dictate the astrocytic dynamics.

Furthermore, distinct from the encoding and retrieval phases, the astrocytic Ca^{2+} dynamics in the hippocampus started to decline immediately after the maintenance phase (in the absence of sensory input) and continued to decline below baseline for up to 20 s, but then remained at the baseline level for the rest of the prolonged delay time (from 20 to 60 s). Meanwhile, neuronal Ca^{2+} remained at the baseline level throughout the maintenance phase.

Entrainment of the Astrocytic and Neuronal Ca^{2+} Dynamics During Information Processing of WM (by Bidirectional and Antagonistic Interaction) with a Characteristic 3-s Phase Difference

The most notable Ca^{2+} patterns were that the astrocytic and neuronal Ca^{2+} dynamics at the population level (i.e., neural and astrocytic ensembles) exhibited inter-locked, antagonistic patterns during the encoding and retrieval phases. Both neuronal and astrocytic Ca^{2+} exhibited an initial rise as an animal approached the turning point of the T-maze, but neuronal Ca^{2+} started to decline after passing the turning point while astrocytic Ca^{2+} continued to rise. Astrocytes express a repertoire of receptors, transporters, and other molecules, enabling them to sense a multitude of synaptic mediators as well as cytokines. The continuing rise after the turning point may be explained by the synaptic release of neurotransmitters which can be sensed by astrocytes, contributing to the continued rise until reaching the reward. On the other hand, the continuous increase in astrocytic Ca^{2+} was closely associated with the decrease in neuronal Ca^{2+}, resulting in the inter-locking of the astrocytic Ca^{2+} peak with the neuronal Ca^{2+} valley. The correlation analysis and hysteresis loop showed both positive and negative correlations between astrocytic and neuronal Ca^{2+} signals, supporting this bidirectional interaction (initially, neurons facilitate astrocytes and then astrocytes inhibit neurons). This antagonistic relationship between the rise of astrocytic Ca^{2+} and decrease of neuronal Ca^{2+} at the population level is in agreement with the similar antagonistic interaction of astrocytes and neurons in response to sensory stimuli [55]. This may involve the release of ATP/adenosine and GABA as gliotransmitters to inhibit synaptically-evoked firing at the surrounding synapses to modify neuronal plasticity [56, 57].

From the dynamic Ca^{2+} patterns, we recorded a neuronal peak at the turning point and an astrocytic peak at the reward delivery point, the neuronal peak preceding the astrocytic peak by ~2–3 s. Conversely, an astrocytic peak preceded a neuronal valley, also by ~2–3 s. These temporal relationships were supported by cross-correlation analysis showing that the phase-difference between the highest positive correlation of the neural and astrocytic Ca^{2+} dynamics as well as the highest negative correlation were both close to 3 s, probably due to the difference between the neuronal signal (15–100 ms) and the astrocytic signal (1–3 s) in response to sensory input [58]. This is consistent with a previous report showing that astrocytic visual responses are delayed by ~ 5 s relative to the surrounding neuronal responses [31]. This delay is apparently caused by the necessity for the total amount of integrated local synaptic activity to exceed a threshold to enable Ca^{2+} responses. On the other hand, the 3-s delay in neuronal Ca^{2+} in association with an increase in astrocytic Ca^{2+} reflects the time during which release of a gliotransmitter acts on neurons to produce an effect at the population level. This is consistent with the previous finding that optogenetic stimulation of astrocytes immediately evokes the blood oxygenation level-dependent signals representing neuronal activation [59]. Thus, neuron–astrocyte interaction at the population level is characterized by a second level of temporal relationship (average 2–3-s phase difference), likely involving the release of neurotransmitters and gliotransmitters in this bidirectional interaction.

Rule-Learning in WM is Associated with Reduced Astrocytic Ca^{2+} Signal During the Retrieval Phases

We also investigated whether learning can produce functional plasticity changes in astrocytic Ca^{2+} patterns by comparing the astrocytic Ca^{2+} dynamics during the correct *versus* wrong trials and by monitoring the dynamics after 4 days of training. The consistent difference between the

correct and wrong trials was a weaker Ca^{2+} signal in the correct trials than in the wrong trials during the retrieval phase. Similarly, population astrocytic and neuronal Ca^{2+} signals during the retrieval phase were reduced on days 3 and 4 compared to day 1. These findings support the idea that rule learning in WM causes functional plasticity in the astrocytic Ca^{2+} dynamics. This decrease of the astrocytic Ca^{2+} dynamics may be a reduction (with modified tuning properties) of the same population or gradual reduction of other neural population activities that are not relevant to WM performance. This finding is consistent with a previous finding of an early expansion of the neuronal populations, followed by a reduction into smaller neuronal population at the proficiency stage during motor and neuroprosthetic learning [60].

Furthermore, rule learning in WM over four days also produced a gradual increase of astrocytic and neuronal Ca^{2+} signals during the maintenance phase of WM. The functional significance of these plasticity changes remains unclear as the hippocampal Ca^{2+} dynamics lack persistent activation during the maintenance in contrast to the PFC. The functional plasticity changes in the hippocampal astrocytic Ca^{2+} dynamics support the involvement of astrocyte population Ca^{2+} signal in the control of WM. This view is consistent with previous findings that astrocytes control WM by modulating the astrocytic release of D-serine to "boost" LTP induction [39], by the astrocyte-derived molecule, L-lactate, that is used as a metabolic fuel to enhance LTP at the hippocampal CA1 synapse [38], and by cannabinoid receptor type-1 signaling *via* inhibition of transmitter release [8]. Astrocytes may also mediate the effects of vigilance and arousal on memory consolidation and performance.

Synchronization and Heterogeneity of Astrocytic Ca^{2+} Signals Responding to WM Processing in Distinct Brain Regions

Synchronization of different brain areas is essential for cognitive performance and sensory perception and is regulated by behavioral demand [47]. The mPFC is considered to be critical to WM processing through persistent neuronal activation during the maintenance phase [36]. Increasing evidence supports the existence of neuronal network interactions between the mPFC and hippocampus during WM processing [42, 45, 47, 61, 62]. These two regions are interconnected by dense monosynaptic and polysynaptic interconnections, and are strongly neurally synchronized [63]. Notably, their synchronization (theta oscillations) is enhanced during the delay and choice periods of WM [64–66]. However, little is known about the dynamic interaction of the astrocytic network between the mPFC and hippocampus during WM processing. In the present study, we showed for the first time the synchronization of population astrocytic responses among WM-related brain regions, especially between the mPFC and hippocampus. We discovered that astrocytic Ca^{2+} activity in the mPFC and hippocampus was closely parallel and locked in phase during the encoding and retrieval phases (especially at the decision-making point), but not at other points (see Fig. 6D), suggesting strong synchronization of the astrocytic network between the two brain regions during WM processing (rather than synchronizing with motor activity which displayed non-phasic pattern). Given the rapid propagation of astrocytic Ca^{2+} waves, this synchronization of the Ca^{2+} dynamics in the mPFC and hippocampus while performing the WM task [42, 61, 67] may be explained by a coordination through astrocytic Ca^{2+} network synchronization.

We also demonstrated the heterogeneity of the dynamic characteristics of astrocytic Ca^{2+} in distinct regions responding to WM processing. Basal astrocytic Ca^{2+} activity in the striatum was much lower than in the mPFC and hippocampus, consistent with a previous study reporting distinct Ca^{2+} homeostasis in striatal and hippocampal astrocytes [48]. These differences in basal astrocytic Ca^{2+} may be attributed to a difference in Ca^{2+} entry into the cell through Ca^{2+}-permeable receptors, Ca^{2+} channels, and Na^{+}/Ca^{2+} exchangers, as well as Ca^{2+} passing through IP3Rs on the endoplasmic reticulum and through the mitochondrial permeability transition pore.

Collectively, our analysis revealed that the dynamics of astrocytic Ca^{2+} are gated not only by sensory inputs (centering at the turning point of the T-maze) but also by the internal state (delivery of the reward) during the sample and choice phases. Importantly, our recordings revealed a strong inter-locked and antagonistic relationship between the astrocytic and neuronal Ca^{2+} dynamics, in which increased neural inputs may trigger astrocyte Ca^{2+} increase, which in turn constrains neuronal activity during WM information processing. This inter-locked relationship between the astrocytic and neuronal Ca^{2+} dynamics during WM information processing is characterized by a temporal pattern with a 3-s phase difference. Furthermore, rule-learning during WM training causes functional plasticity changes in astrocytic Ca^{2+} with a reduced signal during the retrieval phases. Last, we uncovered the synchronization and heterogeneity of astrocytic Ca^{2+} signals responding to WM processing between the hippocampus, mPFC, and striatum. These findings support the existence of bidirectional and inter-locked communication between astrocytes and neurons at the population level during WM information processing, and they work in concert to fine-tune the dynamic range of the stimulus-response relationship according to the sensory inputs and WM performance. As current application of optogenetics to astrocytes usually

does not produce a temporally precise activation of astrocytes (ranging from 10–30 s [68, 69] to 5–15 min [1, 70]), this hampers our ability to dissect a causal role of astrocytes in the distinct phases of WM information processing (i.e., within a few seconds). Future studies are warranted to validate the function of these astrocytic Ca^{2+} patterns by refined optogenetic manipulation of the astrocytic Ca^{2+} dynamics or replay of astrocytic Ca^{2+} patterns.

Acknowledgements This work was supported by Start-up Funds from Wenzhou Medical University (89211010 and 89212012), the National Natural Science Foundation of China (81630040, 31771178, and 81600991), and the Natural Science Foundation of Zhejiang Province of China (LY21H090014 and LQ18C090002).

Conflict of interest The authors claim that there are no conflicts of interest.

References

1. Adamsky A, Kol A, Kreisel T, Doron A, Ozeri-Engelhard N, Melcer T. Astrocytic activation generates de novo neuronal potentiation and memory enhancement. Cell 2018, 174: 59-71.e14.
2. Hasan U, Singh SK. The astrocyte-neuron interface: An overview on molecular and cellular dynamics controlling formation and maintenance of the tripartite synapse. Methods Mol Biol 2019, 1938: 3–18.
3. Martín R, Bajo-Grañeras R, Moratalla R, Perea G, Araque A. Circuit-specific signaling in astrocyte-neuron networks in basal ganglia pathways. Science 2015, 349: 730–734.
4. Martin-Fernandez M, Jamison S, Robin LM, Zhao Z, Martin ED, Aguilar J, *et al*. Synapse-specific astrocyte gating of amygdala-related behavior. Nat Neurosci 2017, 20: 1540–1548.
5. Oliveira JF, Sardinha VM, Guerra-Gomes S, Araque A, Sousa N. Do stars govern our actions? Astrocyte involvement in rodent behavior. Trends Neurosci 2015, 38: 535–549.
6. Robin LM, Oliveira da Cruz JF, Langlais VC, Martin-Fernandez M, Metna-Laurent M, Busquets-Garcia A, *et al*. Astroglial CB_1 receptors determine synaptic D-serine availability to enable recognition memory. Neuron 2018, 98: 935–944.e5.
7. Savtchouk I, Di Castro MA, Ali R, Stubbe H, Luján R, Volterra A. Circuit-specific control of the medial entorhinal inputs to the dentate gyrus by atypical presynaptic NMDARs activated by astrocytes. Proc Natl Acad Sci U S A 2019, 116: 13602–13610.
8. Han J, Kesner P, Metna-Laurent M, Duan TT, Xu L, Georges F, *et al*. Acute cannabinoids impair working memory through astroglial CB_1 receptor modulation of hippocampal LTD. Cell 2012, 148: 1039–1050.
9. Matos M, Shen HY, Augusto E, Wang YM, Wei CJ, Wang YT, *et al*. Deletion of adenosine A2A receptors from astrocytes disrupts glutamate homeostasis leading to psychomotor and cognitive impairment: Relevance to schizophrenia. Biol Psychiatry 2015, 78: 763–774.
10. Ben Menachem-Zidon O, Avital A, Ben-Menahem Y, Goshen I, Kreisel T, Shmueli EM, *et al*. Astrocytes support hippocampal-dependent memory and long-term potentiation via interleukin-1 signaling. Brain Behav Immun 2011, 25: 1008–1016.
11. Tanaka M, Shih PY, Gomi H, Yoshida T, Nakai J, Ando R, *et al*. Astrocytic Ca^{2+} signals are required for the functional integrity of tripartite synapses. Mol Brain 2013, 6: 6.
12. Otte DM, Barcena de Arellano ML, Bilkei-Gorzo A, Albayram O, Imbeault S, Jeung H, *et al*. Effects of chronic D-serine elevation on animal models of depression and anxiety-related behavior. PLoS One 2013, 8: e67131. DOI: https://doi.org/10.1371/journal.pone.0067131.
13. Cao X, Li LP, Wang Q, Wu Q, Hu HH, Zhang M, *et al*. Astrocyte-derived ATP modulates depressive-like behaviors. Nat Med 2013, 19: 773–777.
14. Haydon PG. Astrocytes and the modulation of sleep. Curr Opin Neurobiol 2017, 44: 28–33.
15. Blutstein T, Haydon PG. Chapter Five - The Tripartite Synapse: A Role for Glial Cells in Modulating Synaptic Transmission. The Synapse. 1st ed. Academic Press, 2014: 155–172.
16. Kofuji P, Araque A. G-protein-coupled receptors in astrocyte-neuron communication. Neuroscience 2021, 456: 71–84.
17. Verkhratsky A, Nedergaard M. Physiology of astroglia. Physiol Rev 2018, 98: 239–389.
18. Wang X, Lou N, Xu Q, Tian GF, Peng WG, Han X, *et al*. Astrocytic Ca^{2+} signaling evoked by sensory stimulation *in vivo*. Nat Neurosci 2006, 9: 816–823.
19. Qin H, He WJ, Yang CY, Li J, Jian TL, Liang SS, *et al*. Monitoring astrocytic Ca^{2+} activity in freely behaving mice. Front Cell Neurosci 2020, 14: 603095.
20. Fiacco TA, McCarthy KD. Multiple lines of evidence indicate that gliotransmission does not occur under physiological conditions. J Neurosci 2018, 38: 3–13.
21. Savtchouk I, Volterra A. Gliotransmission: beyond black-and-white. J Neurosci 2018, 38: 14–25.
22. Guerra-Gomes S, Sousa N, Pinto L, Oliveira JF. Functional roles of astrocyte calcium elevations: From synapses to behavior. Front Cell Neurosci 2017, 11: 427.
23. Shigetomi E, Saito K, Sano F, Koizumi S. Aberrant calcium signals in reactive astrocytes: A key process in neurological disorders. Int J Mol Sci 2019, 20: E996.
24. Birkner A, Tischbirek CH, Konnerth A. Improved deep two-photon calcium imaging *in vivo*. Cell Calcium 2017, 64: 29–35.
25. Thrane AS, Rangroo Thrane V, Zeppenfeld D, Lou NH, Xu QW, Nagelhus EA, *et al*. General anesthesia selectively disrupts astrocyte calcium signaling in the awake mouse cortex. Proc Natl Acad Sci U S A 2012, 109: 18974–18979.
26. Descalzi G. Cortical astrocyte-neuronal metabolic coupling emerges as a critical modulator of stress-induced hopelessness. Neurosci Bull 2021, 37: 132–134.
27. Martianova E, Aronson S, Proulx CD. Multi-fiber photometry to record neural activity in freely-moving animals. J Vis Exp 2019, https://doi.org/10.3791/60278.
28. Meng CB, Zhou JH, Papaneri A, Peddada T, Xu KR, Cui GH. Spectrally resolved fiber photometry for multi-component analysis of brain circuits. Neuron 2018, 98: 707-717.e4.
29. Qin H, Lu J, Jin WJ, Chen XW, Fu L. Multichannel fiber photometry for mapping axonal terminal activity in a restricted brain region in freely moving mice. Neurophotonics 2019, 6: 035011.
30. Ung K, Tepe B, Pekarek B, Arenkiel BR, Deneen B. Parallel astrocyte calcium signaling modulates olfactory bulb responses. J Neurosci Res 2020, 98: 1605–1618.
31. Sonoda K, Matsui T, Bito H, Ohki K. Astrocytes in the mouse visual cortex reliably respond to visual stimulation. Biochem Biophys Res Commun 2018, 505: 1216–1222.
32. Ding FF, O'Donnell J, Thrane AS, Zeppenfeld D, Kang HY, Xie LL, *et al*. α1-Adrenergic receptors mediate coordinated Ca^{2+} signaling of cortical astrocytes in awake, behaving mice. Cell Calcium 2013, 54: 387–394.
33. Baddeley A. Working memory. Current Biology 2010, 20: R136–R140.

34. Arnsten AF, Wang MJ, Paspalas CD. Neuromodulation of thought: Flexibilities and vulnerabilities in prefrontal cortical network synapses. Neuron 2012, 76: 223–239.
35. Riga Matos MR, Glas A, Smit AB, Spijker S, van den Oever MC. Optogenetic dissection of medial prefrontal cortex circuitry. Front Syst Neurosci 2014, 8: 230.
36. Liu D, Gu XW, Zhu J, Zhang XX, Han Z, Yan WJ, *et al*. Medial prefrontal activity during delay period contributes to learning of a working memory task. Science 2014, 346: 458–463.
37. Logan S, Pharaoh GA, Marlin MC, Masser DR, Matsuzaki S, Wronowski B, *et al*. Insulin-like growth factor receptor signaling regulates working memory, mitochondrial metabolism, and amyloid-β uptake in astrocytes. Mol Metab 2018, 9: 141–155.
38. Newman LA, Korol DL, Gold PE. Lactate produced by glycogenolysis in astrocytes regulates memory processing. PLoS One 2011, 6: e28427.
39. Henneberger C, Papouin T, Oliet SH, Rusakov DA. Long-term potentiation depends on release of D-serine from astrocytes. Nature 2010, 463: 232–236.
40. Suzuki A, Stern SA, Bozdagi O, Huntley GW, Walker RH, Magistretti PJ, *et al*. Astrocyte-neuron lactate transport is required for long-term memory formation. Cell 2011, 144: 810–823.
41. Jonides J, Lewis RL, Nee DE, Lustig CA, Berman MG, Moore KS. The mind and brain of short-term memory. Annu Rev Psychol 2008, 59: 193–224.
42. Spellman T, Rigotti M, Ahmari SE, Fusi S, Gogos JA, Gordon JA. Hippocampal-prefrontal input supports spatial encoding in working memory. Nature 2015, 522: 309–314.
43. Li ZH, Chen XJ, Wang T, Gao Y, Li F, Chen L, *et al*. The corticostriatal adenosine A_{2A} receptor controls maintenance and retrieval of spatial working memory. Biol Psychiatry 2018, 83: 530–541.
44. Stobart JL, Ferrari KD, Barrett MJP, Glück C, Stobart MJ, Zuend M, *et al*. Cortical circuit activity evokes rapid astrocyte calcium signals on a similar timescale to neurons. Neuron 2018, 98: 726-735.e4.
45. Wirt RA, Hyman JM. Integrating spatial working memory and remote memory: Interactions between the medial prefrontal cortex and hippocampus. Brain Sci 2017, 7: E43.
46. McNab F, Klingberg T. Prefrontal cortex and basal ganglia control access to working memory. Nat Neurosci 2008, 11: 103–107.
47. Churchwell JC, Kesner RP. Hippocampal-prefrontal dynamics in spatial working memory: Interactions and independent parallel processing. Behav Brain Res 2011, 225: 389–395.
48. Chai H, Diaz-Castro B, Shigetomi E, Monte E, Octeau JC, Yu XZ, *et al*. Neural circuit-specialized astrocytes: Transcriptomic, proteomic, morphological, and functional evidence. Neuron 2017, 95: 531-549.e9.
49. Khakh BS, Sofroniew MV. Diversity of astrocyte functions and phenotypes in neural circuits. Nat Neurosci 2015, 18: 942–952.
50. Klink PC, Jeurissen D, Theeuwes J, Denys D, Roelfsema PR. Working memory accuracy for multiple targets is driven by reward expectation and stimulus contrast with different time-courses. Sci Rep 2017, 7: 9082.
51. Paukert M, Agarwal A, Cha J, Doze VA, Kang JN, Bergles DE. Norepinephrine controls astroglial responsiveness to local circuit activity. Neuron 2014, 82: 1263–1270.
52. Schober P, Boer C, Schwarte LA. Correlation coefficients. Anesth Analg 2018, 126: 1763–1768.
53. Oe Y, Wang XW, Patriarchi T, Konno A, Ozawa K, Yahagi K, *et al*. Distinct temporal integration of noradrenaline signaling by astrocytic second messengers during vigilance. Nat Commun 2020, 11: 471.
54. Wikenheiser AM, Redish AD. Decoding the cognitive map: Ensemble hippocampal sequences and decision making. Curr Opin Neurobiol 2015, 32: 8–15.
55. Lines J, Martin ED, Kofuji P, Aguilar J, Araque A. Astrocytes modulate sensory-evoked neuronal network activity. Nat Commun 2020, 11: 3689.
56. Corkrum M, Covelo A, Lines J, Bellocchio L, Pisansky M, Loke K, *et al*. Dopamine-evoked synaptic regulation in the nucleus accumbens requires astrocyte activity. Neuron 2020, 105: 1036-1047.e5.
57. Gaidin SG, Zinchenko VP, Sergeev AI, Teplov IY, Mal'tseva VN, Kosenkov AM. Activation of alpha-2 adrenergic receptors stimulates GABA release by astrocytes. Glia 2020, 68: 1114–1130.
58. Semyanov A, Henneberger C, Agarwal A. Making sense of astrocytic calcium signals - from acquisition to interpretation. Nat Rev Neurosci 2020, 21: 551–564.
59. Takata N, Sugiura Y, Yoshida K, Koizumi M, Hiroshi N, Honda K, *et al*. Optogenetic astrocyte activation evokes BOLD fMRI response with oxygen consumption without neuronal activity modulation. Glia 2018, 66: 2013–2023.
60. Koralek AC, Costa RM, Carmena JM. Temporally precise cell-specific coherence develops in corticostriatal networks during learning. Neuron 2013, 79: 865–872.
61. Tamura M, Spellman TJ, Rosen AM, Gogos JA, Gordon JA. Hippocampal-prefrontal theta-gamma coupling during performance of a spatial working memory task. Nat Commun 2017, 8: 2182.
62. Liu TT, Bai WW, Xia M, Tian X. Directional hippocampal-prefrontal interactions during working memory. Behav Brain Res 2018, 338: 1–8.
63. Cardoso-Cruz H, Paiva P, Monteiro C, Galhardo V. Bidirectional optogenetic modulation of prefrontal-hippocampal connectivity in pain-related working memory deficits. Sci Rep 2019, 9: 10980.
64. Hyman JM, Zilli EA, Paley AM, Hasselmo ME. Working memory performance correlates with prefrontal-hippocampal theta interactions but not with prefrontal neuron firing rates. Front Integr Neurosci 2010, 4: 2.
65. Hallock HL, Wang A, Griffin AL. Ventral midline thalamus is critical for hippocampal-prefrontal synchrony and spatial working memory. J Neurosci 2016, 36: 8372–8389.
66. Johnson EL, Adams JN, Solbakk AK, Endestad T, Larsson PG, Ivanovic J, *et al*. Dynamic frontotemporal systems process space and time in working memory. PLoS Biol 2018, 16: e2004274.
67. Zielinski MC, Shin JD, Jadhav SP. Coherent coding of spatial position mediated by theta oscillations in the hippocampus and prefrontal cortex. J Neurosci 2019, 39: 4550–4565.
68. Octeau JC, Gangwani MR, Allam SL, Tran D, Huang SH, Hoang-Trong TM, *et al*. Transient, consequential increases in extracellular potassium ions accompany Channelrhodopsin2 excitation. Cell Rep 2019, 27: 2249–2261.e7.
69. Perea G, Yang A, Boyden ES, Sur M. Optogenetic astrocyte activation modulates response selectivity of visual cortex neurons *in vivo*. Nat Commun 2014, 5: 3262.
70. Li Y, Li L, Wu J, Zhu Z, Feng X, Qin L, *et al*. Activation of astrocytes in hippocampus decreases fear memory through adenosine A_1 receptors. Elife 2020, 9: e57155.